

To appear in Proc. 10th Pacific-Rim Symposium on Image and Video Technology,
Lecture Notes in Computer Science, Springer, Cham, 2022.

A Wasserstein GAN for Joint Learning of Inpainting and Spatial Optimisation

Pascal Peter

Mathematical Image Analysis Group, Faculty of Mathematics and Computer Science,
Campus E1.7, Saarland University, 66041 Saarbrücken, Germany.
`peter@mia.uni-saarland.de`

Abstract. Image inpainting is a restoration method that reconstructs missing image parts. However, a carefully selected mask of known pixels that yield a high quality inpainting can also act as a sparse image representation. This challenging spatial optimisation problem is essential for practical applications such as compression. So far, it has been almost exclusively addressed by model-based approaches. First attempts with neural networks seem promising, but are tailored towards specific inpainting operators or require postprocessing. To address this issue, we propose the first generative adversarial network (GAN) for spatial inpainting data optimisation. In contrast to previous approaches, it allows joint training of an inpainting generator and a corresponding mask optimisation network. With a Wasserstein distance, we ensure that our inpainting results accurately reflect the statistics of natural images. This yields significant improvements in visual quality and speed over conventional stochastic models. It also outperforms current spatial optimisation networks.

Keywords: inpainting · spatial optimisation · generative adversarial network · Wasserstein distance.

1 Introduction

Image inpainting was originally introduced to restore missing or damaged image parts [6,22]. In this classical setting, the known image data is predetermined. However, given the original image, one can instead consider a spatial optimisation problem: finding a fraction of known data that allows a high quality reconstruction of the image with inpainting. These sparse representations, the so-called inpainting masks, have practical applications such as inpainting-based compression [13,26] and adaptive sampling [11]. Therefore, many sophisticated model-based approaches have been proposed for spatial optimisation of inpainting data [5,7,9,10,15,17,21]. However, due to the unique challenges of this

problem, solutions are often slow, complicated, or limited to specific inpainting operators.

Recently, some first attempts were made to solve the mask optimisation problem with neural networks [1,11]. However, these approaches have limitations. From classical methods it is well known that optimal positions for an inpainting mask heavily depend on the inpainting operator [24]. Despite this close connection, existing deep learning approaches do not allow to train a pair of inpainting and spatial optimisation networks, but either train them separately [11] or do not allow learned inpainting at all [1].

1.1 Our Contribution

We propose the first generative adversarial approach for deep inpainting and spatial optimisation. It consists of three networks: an inpainting generator, a mask generator, and a discriminator. The discriminator allows our learned inpainting to approximate the statistics of natural images in terms of a Wasserstein distance, leading to convincing visual quality. Our mask network is the first to generate binary inpainting masks directly. It solves non-differentiability issues with approaches from neural network-based image compression. The combination of these ingredients makes effective joint learning of inpainting and mask optimisation possible.

1.2 Related Work

The selection of suitable known data is highly dependent on the inpainting operator. Only for individual operators such as homogeneous diffusion [16], true optimality statements have been proven [5], but even those can only be approximated in practice. Optimal control [7,9,15] approaches and a recent finite element method [10] offer good results, but are limited to certain operators. In our comparisons, we consider *probabilistic sparsification* (PS) and *non-local pixel exchange* (NLPE) [21] as representatives for classical methods. PS is a stochastic greedy method that gradually removes pixels which increase the inpainting error the least. NLPE is a postprocessing step which moves mask points to the most promising positions of a randomly chosen candidate set. Together, they belong to the current state of the art in quality and are applicable to any deterministic inpainting operator. For a more detailed review of model-based spatial optimisation, we refer to Alt et al. [1].

To the best of our knowledge, only two deep learning approaches for spatial inpainting data optimisation exist so far. The network of Alt et al. [1] differs fundamentally from our approach in that it optimises masks for homogeneous diffusion inpainting, not for a deep inpainting. During training, the mask network feeds a non-binary confidence map for known data to a surrogate network approximating homogeneous diffusion. It requires postprocessing by stochastic sampling to obtain the final binary masks. The adaptive sampling contribution of Dai et al. [11] is closer in spirit to our approach: It combines a mask network *NetM* with a pre-trained inpainting network *NetE*. The authors note that joint

training of NetM and NetE did not yield satisfying results due the non-binary output of NetM. We address this in more detail in Section 3.1.

A full review of the numerous deep inpainting approaches is beyond the scope of this paper. Most of these [19,20,23,31,32,34,35,36] focus on classical inpainting problems: Regular shaped regions like squares, circles, text, or free form scribbles are removed from the image. Typically this means that only a modest amount of data is missing (10%–60%). In contrast, sparse spatial optimisation is mostly concerned with much higher amounts of unknown data ($> 90\%$) since those are interesting for compression or adaptive sampling purposes. Moreover, optimised known data is often not only extremely sparse, but also does not provide nicely connected regions. Most existing approaches are thus not directly applicable and at the very least, the training procedure must be adapted.

Deep learning methods specifically designed for sparse data are much more rare [28,30]. We explain in more detail in Section 2 why we specifically choose Wasserstein GANs [3,30] as a foundation for our approach. Note that none of the aforementioned pure inpainting methods provides the option for data optimisation or has been previously evaluated on optimised known data.

1.3 Organisation of the Paper

After a brief review of Wasserstein GANs in Section 2 we introduce our deep spatial optimisation approach in Section 3 and evaluate it in Section 4. The paper concludes with a discussion and outlook on future work in Section 5.

2 Inpainting with Wasserstein GANs

For our data optimisation, we require deep inpainting that is suitable for sparse known data. Vařata et al. [30] have successfully applied *Wasserstein generative adversarial networks* (WGANs) for inpainting on random sparse data. Since WGANs are also mathematically well-founded, they are a natural starting point for our approach. In particular, *generative adversarial networks* (GANs) [14] can be seen as generalisation of classical inpainting techniques that achieve high quality [26] by accurately approximating the statistics of natural images [25].

A GAN relies on two competing networks to generate samples from a target distribution \mathbb{P}_t . The *generator* takes a sample from a source distribution \mathbb{P}_s and maps it to a representative of \mathbb{P}_t . In our case, \mathbb{P}_s is a uniformly random distribution, and \mathbb{P}_t corresponds to the statistics of natural images. The *discriminator* judges how well the generated representative fits to the target distribution. This creates a minmax problem, in which the generator tries to trick the discriminator in accepting its result as a true sample of \mathbb{P}_t .

Unfortunately, GANs tend to suffer from training instabilities due to imbalances between the generator and the discriminator. Arjovsky et al. [3] have shown the large impact of the loss function, which measures the difference between generator samples and target distributions. Using a Wasserstein distance

[29] instead of the classical Jensen-Shannon divergence [14] stabilises training, avoids vanishing gradients, and indicates training progress more reliably.

Assume we want to inpaint an image of resolution $m \cdot n$ with k channels with a WGAN [30]. We write its $N := mnk$ pixel values in vector notation as $\mathbf{f} \in \mathbb{R}^N$. Data is known at locations where the confidence function $\mathbf{c} \in [0, 1]^N$ is non-zero, thus providing side information for the generator $\mathbf{g} : (\mathbb{R}^N)^3 \rightarrow \mathbb{R}^N$, a parametric function represented by a network. Representing the known data as $\mathbf{C}\mathbf{f}$ with a masking matrix $\mathbf{C} := \text{diag}(\mathbf{c}) \in \mathbb{R}^{N \times N}$, the generator creates the inpainting result $\mathbf{u} \in \mathbb{R}^N$ based on the inpainting constraint

$$\mathbf{u}(\mathbf{r}, \mathbf{c}, \mathbf{C}\mathbf{f}) := (\mathbf{I} - \mathbf{C})\mathbf{g}(\mathbf{r}, \mathbf{c}, \mathbf{C}\mathbf{f}) + \mathbf{C}\mathbf{f}. \quad (1)$$

The discriminator $d : \mathbb{R}^N \times \mathbb{R}^N \rightarrow \mathbb{R}$ aims to distinguish the distribution of the reconstruction with the known data as side information $\mathbb{P}(\mathbf{u}|\mathbf{c}, \mathbf{C}\mathbf{f})$ from the original distribution $\mathbb{P}(\mathbf{f}|\mathbf{c}, \mathbf{C}\mathbf{f})$, minimising

$$\mathbb{E}_{\mathbf{f} \sim \mathbb{P}_t, \mathbf{c} \sim \mathbb{P}_c} (\mathbb{E}_{\mathbf{r} \sim \mathbb{P}_s} d(\mathbf{u}(\mathbf{r}, \mathbf{c}, \mathbf{C}\mathbf{f}), \mathbf{c}) - d(\mathbf{f}, \mathbf{c})). \quad (2)$$

Here, \mathbf{f} is a sample from the natural image distribution \mathbb{P}_t , \mathbf{c} a random mask from the distribution \mathbb{P}_c , and \mathbf{r} a uniformly random seed. \mathbb{E} denotes the expected value which is estimated in practice via the batch mean. To approximate the Lipschitz property required by the Wasserstein distance, the discriminator weights are normalised to 1 in the 2-norm (see [30]). The generator has a combined loss which weights the discriminator opinion with parameter α against a mean absolute error (MAE) in terms of the 1-norm $\|\cdot\|_1$ that attaches the result to the concrete original image \mathbf{f} :

$$\mathbb{E}_{\mathbf{f} \sim \mathbb{P}_t, \mathbf{r} \sim \mathbb{P}_s, \mathbf{c} \sim \mathbb{P}_c} \left(-\alpha d(\mathbf{u}(\mathbf{r}, \mathbf{c}, \mathbf{C}\mathbf{f}), \mathbf{c}) + \|\mathbf{f} - \mathbf{u}(\mathbf{r}, \mathbf{c}, \mathbf{C}\mathbf{f})\|_1 \right). \quad (3)$$

Vařata et al. [30] use a common hourglass structure for \mathbf{g} that successively subsamples the input data, passes it through a bottleneck and upsamples it again to the output (see \mathbf{g} in Fig. 1(a)). Skip connections forward data between corresponding scales in this hierarchical network. The building blocks of their architecture are visualised in Fig. 1(b)-(d).

Downsampling in the hourglass is performed by *CBlocks* using 3 parallel convolutions with filter size 5×5 , dilation rates 0, 2, and 5, and ELU activation. Their concatenated output is followed by a 2×2 max-pooling, which is the output of the block. Upsampling in *TCBlocks* follows the same principle with transposed convolutions and 2×2 upsampling instead. The parallel dilations increase the influence area of these blocks, which is particularly useful for sparse known data, since it increases the chance to include some reliable pixels in the receptive field of the convolution layers. To restrict the image to the original pixel value range $[0, 1]$, the last transposed convolutional layer has a hard sigmoid activation.

The discriminator follows a simpler downsampling architecture, where *FBlocks* combine 5×5 convolutions (stride 2) with Leaky ReLUs (see d in Fig. 1). For exact details we refer to [30].

additive noise $b(x) = x + \varepsilon$	stochastic rounding $b(x) \in \{0, 1\},$ $P(b(x)=1)=x - \lfloor x \rfloor$	hard rounding $b(x) = \lfloor x + 0.5 \rfloor$
--	--	---

Table 1. Binarisation with Quantisation Operators. Here, ε is chosen uniformly random from $[0, 0.5]$. Among the three different options for binarisation operators [27], we choose hard rounding due to its simplicity and good performance in our practical implementation.

3 Learning Masks with Wasserstein GANs

3.1 Learning Binary Masks

Existing networks [1, 11] produce a non-binary confidence map $\mathbf{c} \in [0, 1]^N$ during training. Dai et al. [11] have identified this as a major roadblock for joint training of an inpainting and mask networks. The known data $\mathbf{C}\mathbf{f}$ obtained in Eq. (1) provides information to the inpainting network that is not available during actual inpainting. Therefore, we need to binarise the mask already during training.

Unfortunately, binarisation is non-differentiable and thus prevents backpropagation. We solve this issue with a *binarisation block* for the last step of our mask generator. In a first step of this block, we apply a transposed convolution with a single channel output, followed by a hard sigmoid activation. We interpret the conversion of this non-binary output $\mathbf{c} \in [0, 1]^N$ into a binary mask $\mathbf{b} \in \{0, 1\}^N$ as an extreme case of quantisation. Such a discretisation of the co-domain restricts the admissible range of values, in our case just 0 and 1.

In deep compression, non-differentiability is often addressed by choosing representatives of the quantisation intervals according to additive random noise [4]. Theis et al. [27] have investigated different quantisation strategies in neural network-based compression and the impact of quantisation perturbations on training (see Table 1). Compared with additive noise and stochastic rounding they found hard rounding to perform the best. Therefore, we round non-binary confidence values c according to $b(c) = \lfloor c + 0.5 \rfloor$. Following the findings of Theis et al., we approximate the gradient of the binarisation layer by the derivative of a simple linear function for backpropagation.

3.2 Joint Learning of Inpainting Operator and Masks

The overall structure of our joint mask and inpainting WGAN is displayed in Fig. 1. Our new *mask generator* \mathbf{m} maps the original $\mathbf{f} \in \mathbb{R}^N$ and a uniformly random seed $\mathbf{r} \in \mathbb{R}^N$ to a binary mask $\mathbf{b} = \mathbf{m}(\mathbf{r}, \mathbf{f})$. The generator \mathbf{g} uses this mask and the known data $\mathbf{B}\mathbf{f} := \text{diag}(\mathbf{b})\mathbf{f}$ as side information to create the inpainting result \mathbf{u} from another random seed. The discriminator loss from Eq. 2 and the generator loss from Eq. 3 ensures that the inpainting respects the statistics of natural images. However, the mask \mathbf{c} is replaced by the output \mathbf{b} of the mask generator.

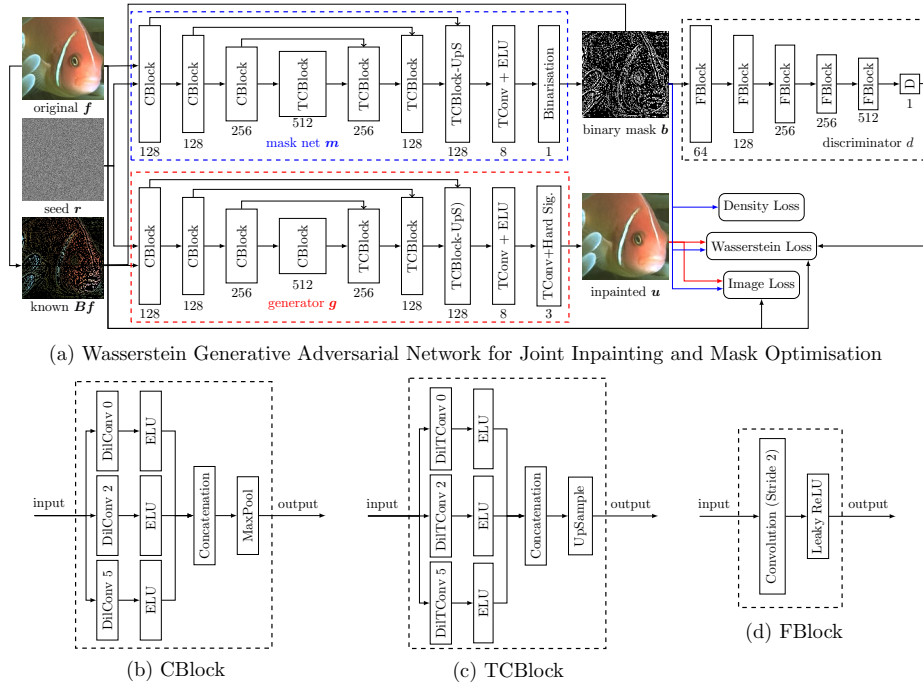


Fig. 1. Overview over our model structure. The arrows denote forward passes. CBlocks, TCBLOCKS, and FBlocks denote convolutional, transposed convolutional, and funnel blocks (see Section 2). The las TCBLOCK omits the upsampling layer (indicated by -UpS). TConv denotes transposed convolutions, DConv dilated convolutions, and DTConv their transposed counterpart. All convolutions use filter size 5×5 . The numbers in dilated convolution layers indicate the dilation parameter. The block height in (a) visualises resolution and the block width roughly indicates the number of output channels, which is precisely given by the numbers below each block.

Unfortunately, we have no way to obtain training data for the unknown distribution of the binary masks that should be approximated by the mask generator m . This distribution depends on the inpainting operator which is simultaneously trained, thus creating a “chicken and egg” problem. We solve this by indirectly describing the distribution: The mask generator is coupled to the Wasserstein loss of the discriminator and generator, since b influences the inpainting result u . Moreover, we define a *density loss* that measures the deviation of percentage of known pixels $\|b\|_1/N$ from the target density D of the inpainting mask. The following loss is directly imposed on the mask network, weighting the density loss against the inpainting MAE by β :

$$\mathbb{E}_{f \sim \mathbb{P}_t, r \sim \mathbb{P}_s} \left(\left| \|\mathbf{m}(r, f)\|_1 / N - D \right| + \beta \|\mathbf{f} - \mathbf{u}(r, \mathbf{m}(r, f), \mathbf{B}f)\|_1 \right). \quad (4)$$

The architecture of the generator and discriminator is identical to the one from Section 2. The mask generator mostly follows the inpainting generator design. We only replace the last block by the binarisation from Section 3.1. Due to the Wasserstein loss, training is straightforward: In each epoch, we update the weights of all three networks with backpropagation. Training remains stable and requires no fine tuning of the balance between generator and discriminator.

4 Experiments

4.1 Experimental Methodology

We compare against state-of-the-art methods for optimisation of inpainting data. As discussed in Section 1.2, most data optimisation techniques are still model-based. Out of the various existing approaches, we choose probabilistic sparsification (PS) and non-local pixel exchange (NLPE) [21], which mark the qualitative state of the art for most inpainting techniques, including the widely-used homogeneous diffusion [16] inpainting. In particular, the diffusion mask network of Alt et al. [1] reaches similar quality as PS on greyscale data. Results on colour images are not available and a corresponding extension would be non-trivial.

Our direct competitor on the neural network side is NetM [11] since it optimises known data for deep inpainting. Therefore, we compare against NetM in combination with all inpainting operators evaluated by Dai et al.- [11]. The numerous pure neural networks for inpainting discussed in Section 1.2 only perform inpainting of pre-defined masks and do not perform spatial optimisation. They can therefore not be considered for comparison.

Our neural networks were trained on the same 100,000 image *ImageNet* subset also used by Dai et al. [11] and the corresponding validation set. Depending on the evaluation set, these were centre-cropped to either 128×128 or 64×64 . We used the *Adam* optimiser [18] with learning rate $5 \cdot 10^{-5}$ and a batch size of $b = 32$ for image size 128×128 , and $b = 128$ for image size 64×64 . The model parameters were set to $\alpha = 0.005$ and $\beta = 1$. For each mask density D , separate networks were trained. We chose the best weights w.r.t. the mask validation loss from Eq. (4) after 1000 epochs. In most cases, this was already reached after roughly 100 epochs.

As evaluation datasets we use the ImageNet test set provided by Dai et al. [11] for the network comparison. For the comparison with NLPE, we use the Berkeley shape database *BSDS500* [2], since it has better public availability and this also demonstrates that our networks transfer well to other natural image databases.

4.2 Comparison Against NetM

We compare against the mask generator NetM [11] on the test set curated by Dai et al. It consists of 1000 images or resolution 64×64 . They provide peak-signal-to-noise ratio (PSNR) results of NetM in combination with the corresponding

Density	(a) random masks		(b) optimised NetM masks				Our MG
	NetE [11]	WGAN [30]	NetE [11]	CDD [8]	BPFA [37]	MS [12]	
5%	18.44	18.85	20.35	20.22	15.82	20.70	21.66
10%	19.94	20.78	21.93	22.42	20.82	22.98	23.63
20%	22.06	22.95	24.31	24.38	24.16	25.04	25.36

Table 2. PSNR Comparison Against NetM on ImageNet (higher is better). Our MG approach outperforms NetM in combination with all four inpainting operators investigated by Dai et al. [11]. In particular, it outperforms the full network approach with NetE consistently by more than 1dB in PSNR, even though MG does not maximise PSNR.

inpainting network NetE and multiple classical inpainting approaches [8,12,37]. Note that NetM is trained to minimise a 2-norm, giving it an advantage over our 1-norm/Wasserstein trained MG in this evaluation. Nevertheless, in Table 2(b), MG outperforms NetM+NetE substantially by up to 1.7 dB.

To verify that this advantage does not only result from using a GAN for inpainting, we also compare the inpainting WGAN [30] to NetE on random masks in Table 2(a). On 5% known data, the WGAN outperforms NetE only by 0.4 dB. Our mask GAN increases this improvement over NetM+NetE to 1.3 dB. This indicates that our mask binarisation and joint training offers an advantage.

Additional inpainting operators in combination with NetM, such as the Bayesian beta process factor analysis (BPFA) [37], curvature-driven diffusion (CCD) [8], or Mumford-Shah (MS) inpainting [12] all yield worse results than our mask GAN. We outperform the best NetM approach by up to 0.96 dB.

4.3 Comparison Against Probabilistic Methods

Probabilistic sparsification (PS) with a non-local pixel exchange (NLPE) as a postprocessing step defines a benchmark for the best results obtainable so far with homogeneous diffusion inpainting. Other methods [1,5,7,9,15] yield comparable or worse quality.

We optimise the stochastic models for mean average error (MAE) since this is also part of the network loss. NLPE uses 5 cycles of $|c|$ iterations. At first glance, in terms of MAE, our mask GAN (MG) is situated between PS and PS+NLPE in Table 3(a). It performs better on sparser masks which are more relevant for e.g. compression applications and comes very close to the NLPE error for 5%. We also evaluate w.r.t. the popular structural-similarity index (SSIM) [33] in Table 3(b). It yields a slightly different ranking, with our mask GAN also outperforming PS+NLPE on the 5% density and very similar values for all methods on 10%.

Since these error measures yield less clear quantitative results than our first set of experiments, we also provide multiple visual examples. Fig. 2 demonstrates that our MG excels for low densities which are useful for applications such as thumbnail compression or destructive image acquisition. This holds especially

Density	(a) MAE (lower is better)			(b) SSIM (higher is better)		
	PS	PS+NLPE	Our MG	PS	PS+NLPE	Our MG
5%	13.98	10.98	11.19	0.69	0.70	0.71
10%	9.08	7.51	8.87	0.80	0.81	0.79
20%	5.19	4.31	6.70	0.90	0.91	0.85

Table 3. Quantitative Comparison to Stochastic Methods on BSDS500.
 (a) W.r.t. MAE, our mask GAN (MG) outperforms probabilistic sparsification (PS) consistently and is competitive with non-local pixel exchange (NLPE) on low densities. (b) In terms of SSIM, at low densities the mask GAN slightly outperforms both competitors while remaining competitive for higher densities at significantly reduced computational load (see Table 4).

for complex images, for instance the high contrast texture of the zebra, or the house with many small-scale details like the lawn and fence. PS and NLPE need to cluster known data left and right to edges according to the optimality theory of Belhachmi et al. [5]. In regions where this is not possible, they suffer from detail loss and colour bleeding. Sometimes, minimising the MAE with NLPE even leads to a slight deterioration w.r.t. SSIM, since some edges are reinforced while others vanish (see Fig. 2(a) and Fig. 2(b)). In contrast, our approach can reconstruct structural image features from less known data. Therefore, it can distribute the mask pixels much more evenly.

These advantages are less pronounced for higher densities or simpler images. With higher amounts of known data, homogeneous diffusion can reconstruct more edges and all approaches become more similar w.r.t. quality. While the MAE and SSIM scores for high densities are slightly worse on average for our mask GAN in Table 3, its visual quality is competitive. The Wasserstein loss does not lead to the smallest possible quantitative errors, but yields natural looking inpainting results in Fig. 3. In particular, our mask approach does not suffer from the visually unpleasant singularities of homogeneous diffusion inpainting that are clearly visible in Fig. 3(a). Here we can also observe that its more even error distribution often leads to better representations of visually important image content such as faces.

In addition to its competitive visual quality, our Mask GAN is substantially faster than a PS/NLPE conjugate-gradient implementation with relative residual 10^{-6} . On a single CPU core, the speed-up reaches up to a factor ≈ 63 w.r.t. PS and a factor ≈ 419 w.r.t. NLPE. With GPU support, our GAN can be up to $\approx 12,560$ times faster. Faster model-based alternatives to PS exist [5,10], but so far, they typically require postprocessing to reach the quality of PS+NLPE. Since they use homogeneous diffusion, they also suffer from visual artefacts like singularities. Overall, our network provides a fast solution for sparse data optimisation with a high visual quality.

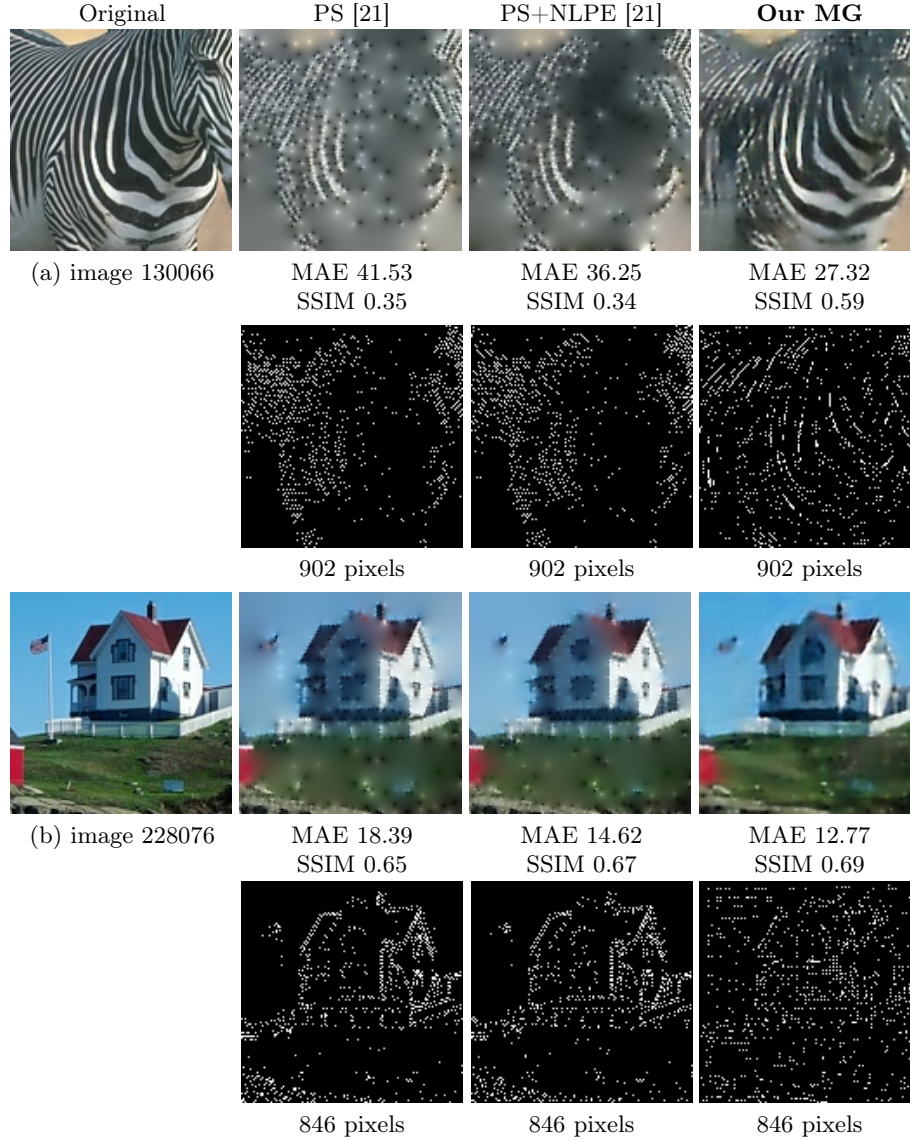


Fig. 2. Visual Comparison to Probabilistic Methods at $\approx 5\%$ Density on BSDS500. Known data points are marked in white. At this extreme density that might be used for e.g. thumbnail compression or destructive image acquisition, our mask WGAN reconstructs structures from less clustered data. It does not suffer from visual artefacts such as singularities or extreme colour bleeding as PS and NLPE with homogeneous diffusion.

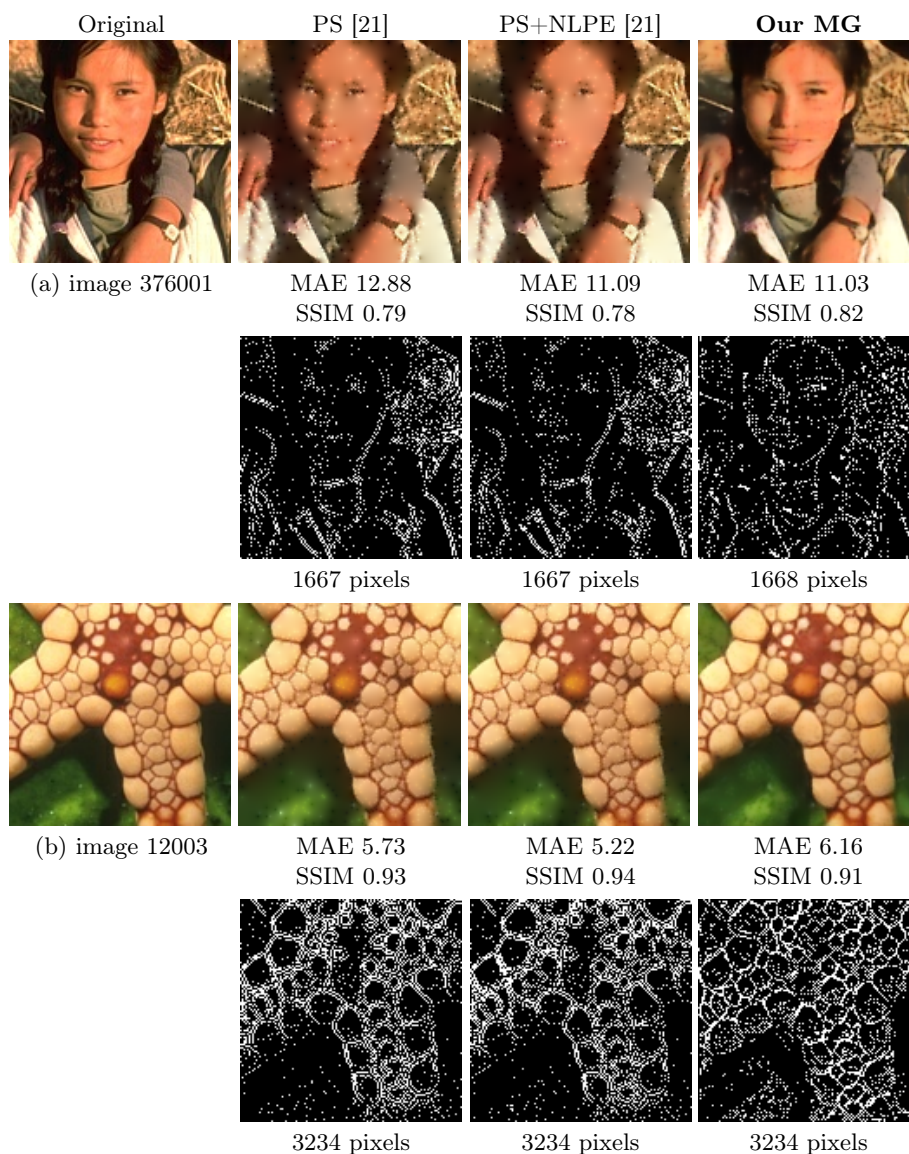


Fig. 3. Visual Comparison to Probabilistic Methods at 10% and 20% on BSDS500. Known data points are marked in white. With increasing density, the quality of all three methods approaches each other. In (a), our MG still benefits from better known data distribution, yielding a more detailed representation of the face. In (b), it produces a similar visual quality as PS and NLPE at a higher error. It does not suffer from singularities, but this is less notable since the quality is overall high.

Density	PS	PS+NLPE	Our MG (CPU)	Our MG (GPU)
5%	58.84	251.28	0.93	0.031
10%	33.89	340.61	0.93	0.031
20%	18.86	389.34	0.93	0.031

Table 4. Runtime Comparison on 128×128 images with an Intel Core i56660K@3.50GHz and a NVIDIA Geforce GTX 1070. Our WGAN is faster than classical methods by several orders of magnitude (factor > 400 on CPU or $> 12,000$ on GPU). Its runtime is independent of the mask density.

5 Conclusion and Future Work

We have presented the first adversarial network for joint learning of a generative inpainting operator and a binary mask generator. Based on a mathematically well-founded Wasserstein framework, our inpainting GAN approximates the statistics of natural images, yielding visual improvements over model-based stochastic approaches with homogeneous diffusion. Simultaneously, our approach is faster by several orders of magnitude. It also qualitatively outperforms competing neural networks for spatial optimisation in combination with many inpainting operators.

Currently, we are working on further refinements of both the general framework and the concrete network architecture. Moreover, we plan to evaluate the impact of individual components with an extended evaluation and ablation study in the future. Our model is a step towards fast, visually accurate, and mathematically justified spatial optimisation with deep learning. We hope that it contributes to practical applications such as image compression or adaptive sampling in the future.

Acknowledgements This work has received funding from the European Research Council (ERC) under the European Union’s Horizon 2020 research and innovation programme (grant agreement no. 741215, ERC Advanced Grant IN-COVID). We thank Dai et al. [11] for providing their reference dataset.

References

1. Alt, T., Peter, P., Weickert, J.: Learning sparse masks for diffusion-based image inpainting. In: Pinho, A.J., Georgieva, P., Teixeira, L.F., Sánchez, J.A. (eds.) Pattern Recognition and Image Analysis, Lecture Notes in Computer Science, vol. 13256, pp. 528–239. Springer, Cham (2022)
2. Arbelaez, P., Maire, M., Fowlkes, C., Malik, J.: Contour detection and hierarchical image segmentation. *IEEE Transactions on Pattern Analysis and Machine Intelligence* **33**(5), 898–916 (Aug 2011)
3. Arjovsky, M., Chintala, S., Bottou, L.: Wasserstein generative adversarial networks. In: Precup, D., Teh, Y.W. (eds.) Proc. 34th International Conference on Machine Learning. Proceedings of Machine Learning Research, vol. 70, pp. 214–223. Sydney, Australia (Aug 2017)

4. Ballé, J., Laparra, V., Simoncelli, E.P.: End-to-end optimised image compression. In: Proc. 5th International Conference on Learning Representations. Toulon, France (Apr 2017)
5. Belhachmi, Z., Bucur, D., Burgeth, B., Weickert, J.: How to choose interpolation data in images. *SIAM Journal on Applied Mathematics* **70**(1), 333–352 (Jun 2009)
6. Bertalmio, M., Caselles, V., Masnou, S., Sapiro, G.: Inpainting. In: Ikeuchi, K. (ed.) *Computer Vision: A Reference Guide*, pp. 401–416. Springer, New York (2014)
7. Bonettini, S., Loris, I., Porta, F., Prato, M., Rebegoldi, S.: On the convergence of a linesearch based proximal-gradient method for nonconvex optimization. *Inverse Problems* **33**(5), article 055005 (Mar 2017)
8. Chan, T.F., Shen, J.: Non-texture inpainting by curvature-driven diffusions (CDD). *Journal of Visual Communication and Image Representation* **12**(4), 436–449 (May 2001)
9. Chen, Y., Ranftl, R., Pock, T.: A bi-level view of inpainting-based image compression. In: Kúkelová, Z., Heller, J. (eds.) Proc. 19th Computer Vision Winter Workshop. Křtiny, Czech Republic (Feb 2014)
10. Chizhov, V., Weickert, J.: Efficient data optimisation for harmonic inpainting with finite elements. In: Tsapatsoulis, N., Panayides, A., Theo, T., Lanitis, A., Pattichis, C. (eds.) *Computer Analysis of Images and Patterns, Lecture Notes in Computer Science*, vol. 13053, pp. 432–441. Springer, Cham (2021)
11. Dai, Q., Chopp, H., Pouyet, E., Cossairt, O., Walton, M., Katsaggelos, A.K.: Adaptive image sampling using deep learning and its application on X-Ray fluorescence image reconstruction. *IEEE Transactions on Multimedia* **22**(10), 2564–2578 (Dec 2019)
12. Esedoglu, S., Shen, J.: Digital inpainting based on the Mumford–Shah–Euler image model. *European Journal of Applied Mathematics* **13**(4), 353–370 (Aug 2002)
13. Galić, I., Weickert, J., Welk, M., Bruhn, A., Belyaev, A., Seidel, H.P.: Image compression with anisotropic diffusion. *Journal of Mathematical Imaging and Vision* **31**(2–3), 255–269 (Jul 2008)
14. Goodfellow, I., Pouget-Abadie, J., Mirza, M., Xu, B., Warde-Farley, D., Ozair, S., Courville, A., Bengio, Y.: Generative adversarial nets. *Advances in Neural Information Processing Systems* **27**, 2672–2680 (Dec 2014)
15. Hoeltgen, L., Setzer, S., Weickert, J.: An optimal control approach to find sparse data for Laplace interpolation. In: Heyden, A., Kahl, F., Olsson, C., Oskarsson, M., Tai, X.C. (eds.) *Energy Minimisation Methods in Computer Vision and Pattern Recognition, Lecture Notes in Computer Science*, vol. 8081, pp. 151–164. Springer, Berlin (2013)
16. Iijima, T.: Basic theory on normalization of pattern (in case of typical one-dimensional pattern). *Bulletin of the Electrotechnical Laboratory* **26**, 368–388 (1962), in Japanese
17. Karos, L., Bheed, P., Peter, P., Weickert, J.: Optimising data for exemplar-based inpainting. In: Blanc-Talon, J., Helbert, D., Philips, W., Popescu, D., Scheunders, P. (eds.) *Advanced Concepts for Intelligent Vision Systems, Lecture Notes in Computer Science*, vol. 11182, pp. 547–558. Springer, Cham (2018)
18. Kingma, D.P., Ba, J.: Adam: A method for stochastic optimization. In: Proc. 3rd International Conference on Learning Representations. San Diego, CA (May 2015)
19. Liu, G., Reda, F.A., Shih, K.J., Wang, T.C., Tao, A., Catanzaro, B.: Image inpainting for irregular holes using partial convolutions. In: Ferrari, V., Herbert, M., Sminchisescu, C., Weiss, Y. (eds.) *Computer Vision – ECCV 2018, Lecture Notes in Computer Science*, vol. 11205, pp. 85–100. Springer, Cham (2018)

20. Liu, H., Jiang, B., Xiao, Y., Yang, C.: Coherent semantic attention for image inpainting. In: Proc. 2019 IEEE/CVF International Conference on Computer Vision. pp. 4170–4179. Seoul, Korea (Oct 2017)
21. Mainberger, M., Hoffmann, S., Weickert, J., Tang, C.H., Johannsen, D., Neumann, F., Doerr, B.: Optimising spatial and tonal data for homogeneous diffusion inpainting. In: Bruckstein, A.M., ter Haar Romeny, B., Bronstein, A.M., Bronstein, M.M. (eds.) Scale Space and Variational Methods in Computer Vision, Lecture Notes in Computer Science, vol. 6667, pp. 26–37. Springer, Berlin (2012)
22. Masnou, S., Morel, J.M.: Level lines based disocclusion. In: Proc. 1998 IEEE International Conference on Image Processing. vol. 3, pp. 259–263. Chicago, IL (Oct 1998)
23. Pathak, D., Krähenbühl, P., Donahue, J., Darrell, T., Efros, A.A.: Context encoders: Feature learning by inpainting. In: Proc. 2016 IEEE Conference on Computer Vision and Pattern Recognition. pp. 2536–2544. Las Vegas, NV (Jun 2016)
24. Peter, P., Hoffmann, S., Nedwed, F., Hoeltgen, L., Weickert, J.: Evaluating the true potential of diffusion-based inpainting in a compression context. *Signal Processing: Image Communication* **46**, 40–53 (Aug 2016)
25. Peter, P., Weickert, J.: Justifying tensor-driven diffusion from structure-adaptive statistics of natural images. In: Tai, X.C., Bae, E., Chan, T.F., Leung, S.Y., Lysaker, M. (eds.) Energy Minimisation Methods in Computer Vision and Pattern Recognition, Lecture Notes in Computer Science, vol. 8932, pp. 263–277. Springer, Berlin (2015)
26. Schmaltz, C., Peter, P., Mainberger, M., Ebel, F., Weickert, J., Bruhn, A.: Understanding, optimising, and extending data compression with anisotropic diffusion. *International Journal of Computer Vision* **108**(3), 222–240 (Jul 2014)
27. Theis, L., Shi, W., Cunningham, A., Huszár, F.: Lossy image compression with compressive autoencoders. In: Proc. 5th International Conference on Learning Representations. Toulon, France (Apr 2016)
28. Ulyanov, D., Vedaldi, A., Lempitsky, V.: Deep image prior. In: Proc. 2018 IEEE Conference on Comp. Vis. and Pattern Recognition. pp. 9446–9454. Salt Lake City, UT (Jun 2018)
29. Vaserstein, L.N.: Markov processes over denumerable products of spaces, describing large systems of automata. *Problemy Peredachi Informatsii* **5**(3), 64–72 (Feb 1969)
30. Vařata, D., Halama, T., Friedjungová, M.: Image inpainting using Wasserstein generative adversarial imputation network. In: Proc. 30th International Conference on Artificial Neural Networks. pp. 575–586 (Sep 2021)
31. Wang, N., Zhang, Y., Zhang, L.: Dynamic selection network for image inpainting. *IEEE Transactions on Image Processing* **30**, 1784–1798 (Jan 2021)
32. Wang, W., Zhang, J., Niu, L., Ling, H., Yang, X., Zhang, L.: Parallel multi-resolution fusion network for image inpainting. In: Proc. 2021 IEEE/CVF International Conference on Computer Vision. pp. 14559–14568 (Oct 2021)
33. Wang, Z., Bovik, A.C., Sheikh, H.R., Simoncelli, E.P.: Image quality assessment: From error visibility to structural similarity. *IEEE Transactions on Image Processing* **13**, 600–612 (Apr 2004)
34. Xie, J., Xu, L., Chen, E.: Image denoising and inpainting with deep neural networks. In: Proc. 26th International Conference on Neural Information Processing Systems. pp. 350–358. Lake Tahoe, NV (Dec 2012)
35. Yu, J., Lin, Z., Yang, J., Shen, X., Lu, X., Huang, T.S.: Free-form image inpainting with gated convolution. In: Proc. 2019 IEEE/CVF International Conference on Computer Vision. pp. 4471–4480. Seoul, Korea (Oct 2019)

36. Yu, T., Guo, Z., Jin, X., Wu, S., Chen, Z., Li, W., Zhang, Z., Liu, S.: Region normalization for image inpainting. In: Proc. AAAI Conference on Artificial Intelligence. vol. 34, pp. 12733–12740. New York, NY (Feb 2020)
37. Zhou, M., Chen, H., Paisley, J., Ren, L., Li, L., Xing, Z., Dunson, D., Sapiro, G., Carin, L.: Nonparametric Bayesian dictionary learning for analysis of noisy and incomplete images. *IEEE Transactions on Image Processing* **21**(1), 130–144 (Jan 2011)